The International Archives of the Photogrammetry, Remote Sensing and Spatial Information Sciences, Volume XLVIII-1/W6-2025
3rd International Workshop on Evaluation and BENCHmarking of Sensors, Systems and
GEOspatial Data in Photogrammetry and Remote Sensing (GEOBENCH), 20–21 November 2025, Wroclaw, Poland

Procedure and Accuracy Assessment Results of Livox MID-360 Scanners

Batosz Mitka[1], Przemysław Klapa[2]

[1]Dep. of Rural Land Surveying, Cadastre and Photogrammetry, University of Agriculture in Krakow, Krakow, Poland – bartosz.mitka@urk.edu.pl
[2]Dep. of Geodesy, University of Agriculture in Krakow, Krakow, Poland – przemyslaw.klapa@urk.edu.pl

Keywords: LiDAR, Livox MID-360, Accuracy assessment, Point cloud analysis, Low-cost laser scanners.

Abstract

Scanning systems, both stationary and mobile, increasingly employ low-cost laser scanners that offer distance measurement accuracy on the order of 1–2 cm with ranges up to several tens of meters. This paper presents a validated, replicable procedure for assessing the accuracy of scanning heads. Results are presented for 35 Livox MID-360 heads.
Measurements were carried out in the laboratory of the Faculty of Environmental Engineering and Geodesy at the University of Agriculture in Krakow. Data acquisition included six angular poses per head; for each pose, three sets of 2 million points were combined (6 million in total). The evaluation included registration to a TLS reference point cloud (Leica P40), Cloud-to-Cloud comparison with decomposition into X/Y/Z components, assignment of a local coordinate system and rasterization with a 0.25 m grid, followed by analysis of the dependence of errors on distance.
The results confirm that measurement errors fall within the manufacturer-declared range for all examined units, indicating the suitability of the heads for centimeter-precision tasks. At the same time, a small step-like change in error in the Z direction was observed at a distance of approximately 10–12 m from the scanner, as well as minor direction-dependent differences in the distributions in the X and Y directions. The proposed procedure provides practical recommendations for quality control, and the obtained results may serve as a reference point for calibration and deployment of low-cost scanners in 3D scanning systems.

1. Instruction.

In recent years, alongside precise, high-resolution spatial scanning systems, smaller and cheaper solutions have emerged, intended mainly for autonomous vehicles and robotics. Their development is driven by growing demand for low-cost systems capable of delivering three-dimensional spatial information in real time. These devices increasingly serve as primary sensors in mapping systems, both stationary and mobile. They are also integrated with unmanned aerial vehicle platforms for acquiring 3D data (Mitka et al. 2024). An example of such solutions is the Livox MID-360 scanning head, a compact three-dimensional laser scanner with non-repetitive scanning, providing a full field of view of 360 degrees horizontally and from −7° to 52° vertically, and a dense point cloud in real time (https://www.livoxtech.com/mid-360).

Livox Mid-360 is a 905-nanometer three-dimensional laser scanner for automated vehicles, robotics, and urban systems; it supports mapping, positioning, and obstacle detection and avoidance, and detects objects from 0.1 meter to 100 meters. The point cloud is acquired by an opto-mechanical system with a rotating mirror and a non-repetitive scanning pattern, which increases scene density and coverage over time (Fig. 1a). The scanning range is 40 m for 10% reflectance and up to 70 m for 80%. Key accuracy parameters are: random distance error ≤ 2 cm at 10 m (up to 3 cm at 0.2 m) and angular error ≤ 0.15°. The scanner generates about 200 thousand points per second at 10 Hz, and data are output via a 100 Mb/s network port. The built-in inertial module with a three-axis accelerometer and gyroscope provides measurements at 200 Hz. The housing has IP67 sealing and allows operation from −20 to 55 °C; the device meets vibration test requirements. Power supply is 9–27 V DC with a typical consumption of 6.5 W, dimensions 65 × 65 × 60 mm, mass about 265 g. The manufacturer, LIVOX, provides software for viewing and analyzing point clouds and for calibration (Livox Viewer), as well as a software development kit and drivers for the Robot Operating System environment, which simplifies building custom applications and integration with robots. Livox Mid-360 uses non-repetitive scanning (Fig. 1b), therefore field-of-view coverage increases with scanning time and successive scene details are revealed; examples for 0.1–1 second show clear densification of the point cloud (Fig. 1c) (Livox Mid-360, User Manual v1.2, 2024; https://www.livoxtech.com/mid-360).

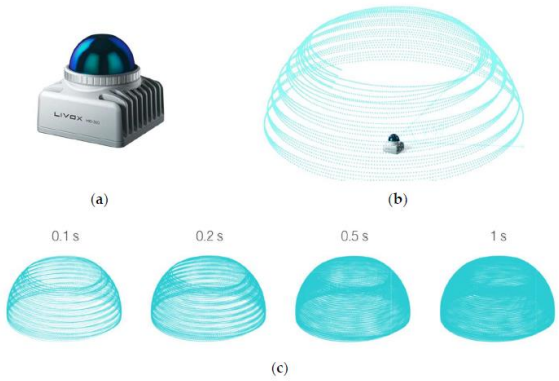

Figure 1. Livox Mid-360: (a) sensor unit; (b) scanning process; (c) point-cloud patterns accumulated over different integration times [Livox Mid-360 User Manual, v1.2, 2024].

The sensor has repeatedly been used and tested by various companies and institutions. Measurements of the properties of low-cost lidars—such as accuracy, data density, noise level, and artifacts—are increasingly being reported. For example, Ortiz Arteaga and co-authors evaluated the performance of the low-cost automotive lidar Livox Mid-40 by analyzing distance measurement, repeatability, and accuracy; the conclusions indicate suitability for “reality capture” tasks, including sketch as-built plans and volume calculations, with reference to the

Leica RTC 360 benchmark scanner (Ortiz et al. 2019). Calibration and stability studies for scanners of this class have been described, among others, for the Velodyne VLP-16 model (Glennie et al. 2016), and a methodology for the metrological assessment of low-cost mobile scanners (using Livox Mid-40 and Ouster OS1-64 as examples) was presented in "Accuracy assessment and calibration of low-cost autonomous lidar sensors," with reference data from the Riegl VZ-2000 (Glennie and Hartzell, 2020). Livox MID-360 is described as a low-cost scanner because it is relatively inexpensive. In paper Bendkowski et al. (2025) it was referred to as "currently the cheapest available LiDAR." The authors used it to demonstrate calibration and synchronization of a camera–LiDAR configuration. The trade literature also widely discusses the calibration and integration of low-cost scanners with inertial units and other sensors in terms of trajectory adjustment accuracy (Wu et al. 2023), (Glennie, 2012) and the quality of acquired geometric data and volume calculations (Hyyppä et al. 2020), (Hu et al. 2021). Livox MID-360 is a hybrid solid-state LiDAR intended mainly for service robots, with an IP67 housing resistant to dust and short-term immersion; the scanning head is used in popular, readily available systems, including for scanning caves and mines (Redovniković et al. 2024). Issues related to SLAM algorithms for low-cost sensors with a small field of view are described, among others, in (Lin and Zhang, 2020; Wang et al. 2021).

Livox MID-360, used among others as a key 3D sensor in the handheld, low-cost MandEye scanner, was subjected to metrological tests in static and dynamic conditions with reference to the TLS cloud Leica ScanStation P40. Sampling and the densification effect resulting from non-repetitive scanning were evaluated: a single cycle provided angular sampling of about 3.0° vertically and 3.5° horizontally, and after 1 second of static scanning, centimeter linear resolutions were obtained for distances of 6–13 m; target identification effectiveness was 88% (0–5 m, static mode) and 31% (dynamic mode), and the fit to TLS was burdened with a mean error of ±0.013 m (static) and ±0.017 m (dynamic). For context, parameters from the documentation were cited: 905 nm, eye-safety class 1, field of view 360°×59°, 200 thousand pts/s at 10 Hz. (Mitka et al. 2024). Livox MID-360, used as a sensor in a low-cost mobile scanning system (LC-MLS), is also increasingly employed in environmental studies and applications, including forest inventory; about 200 thousand pts/s were recorded, ranges up to 70 m were achieved for high reflectance (practically 30–35 m in the forest), with coverage of 360° horizontally and −7° to 52° vertically, on a platform based on Raspberry Pi 4, open-source SLAM algorithms, and export to .LAS/.ply/.e57. The results were compared with TLS and two commercial MLS, obtaining for DBH a bias of +1.62 cm and RMSE of 2.20 cm, and for tree heights a bias of −2.16 m and RMSE of 2.47 m. (Balestra et al., 2024).

2. Methodology of the conducted work

The study presents the accuracy assessment procedure and its results for 35 low-cost laser scanner heads Livox MID 360 (Fig. 2).

Figure 2. Livox MID360 heads (35 units) tested in the study.

The tests were carried out in the measurement laboratory of the Faculty of Environmental Engineering and Geodesy, University of Agriculture in Krakow. For the purposes of the study, a spatial test field was prepared in the laboratory room measuring 37.40 m in length, 6.78 m in width, and 4.22 m in height, with 48 black-and-white measurement targets arranged on the walls and ceiling. This field consisted, in addition to the room with targets itself, of additional targets and reference spheres placed in space at a short distance (up to 2 m) from the station for testing the scanning heads (Fig. 3). The intention was to enable identification of reference points on the point clouds acquired by the Livox MID360 scanners.

Figure 3. Test field and location of the measurement station.

2.1. Measurement data acquisition

The reference measurement of the test field was performed using the Leica P40 terrestrial laser scanner, and the point cloud from this scanner, due to its accuracy, density, and quality of geometric representation, served as the reference for the data from the Livox MID 360 heads.

The measurement setup consisted of a professional surveying tripod mounted on a stable photogrammetric turntable and a dedicated 3D-printed mounting cradle. The scanning head was seated in a cradle dimensioned to its outline, which ensured secure support, repeatable positioning, and stable coupling with the tripod. The cradle functioned as a holder–base: it immobilized the head and at the same time allowed convenient routing of cables and connection to the control system. The

turntable was rotated by specified angles, enabling a series of static measurements for all Livox heads while maintaining constant geometry and the absence of significant vibrations. The entire structure was rigid and stable, which provided metrological conditions for assessing the operating parameters of the heads (Fig. 4). Around the station, reference spheres and photogrammetric targets were arranged in various directions and at different heights. They were used to provide a common orientation to the measurement sets and as control and verification points. Their positions were determined in the laboratory reference frame and used in all test series.

Figure 4. Presentation of the head in the holder on the rotary platform

For each examined head, six angular settings with a 30° rotation (three 10° "clicks" of the turntable) were performed. In each setting, 3 sets of 2,000,000 points were recorded, i.e., a total of 6,000,000 points per measurement. The duration of a single set resulted from reaching a volume of 2 million points (≈10 s at a rate of 200,000 pts/s), and the entire setting was obtained by merging three sets; additionally, merges of two sets were analyzed as a quality-control variant.

Each single measurement set was saved in *.las format, and then composite clouds were created per setting and per head; in total, 210 *.las files were obtained from the Livox heads. For validation, an independent reference cloud from the Leica ScanStation P40 scanner was prepared, which made it possible to compare accuracy and point density under identical geometric conditions.

2.2. Data processing workflow – Accuracy assessment of the geometry of the acquired point clouds

The first stage of data processing involved checking geometric consistency for all heads in all angular poses. For each angular pose, three sets of 2 000 000 points were merged into a single 6 000 000-point cloud. Geometric consistency was verified and confirmed in the CloudCompare software.

The next stage of data processing involved assessing geometric accuracy with respect to the reference cloud from the Leica P40 scanner. The analysis was performed on a sample of 40 *.las files: all rotations for one head and one measurement with the next angle for the remaining heads. The data were then imported into Leica Cyclone, the Livox clouds were registered to the P40 reference cloud, and reports with accuracy parameters were saved. Pairs of clouds (reference and tested) were reloaded into CloudCompare, the transformation from the Cyclone report was applied, and a local coordinate system with axes parallel to the walls was assigned (X to the longer walls, Y to the shorter). The Cloud-to-Cloud distance was computed with separation into X, Y, Z without additional parameters. The clouds were cleaned to homogeneous wall and ceiling planes by removing noise and artifacts. For each wall and the ceiling, rasterization with a 0.25 cell size was performed and the "C2C distance" scalar was selected separately for X, Y, Z. The rasterization results were saved to text files. Finally, plots were created of the relationship between the distance of a point from the Livox MID-360 head and the deviations between the reference and tested clouds, and the results were analyzed. The data processing scheme is presented in graphic form (Fig. 5).

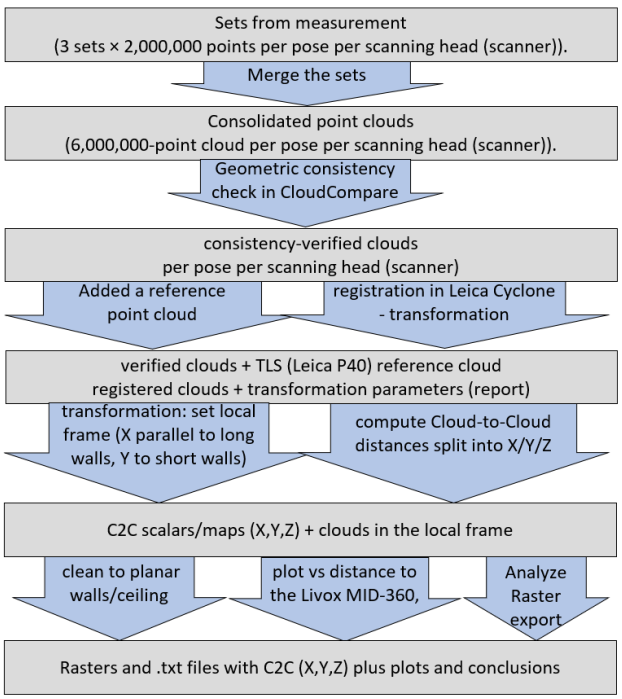

Figure 5. Data processing scheme.

2.3. Study implementation

The study began with data consolidation: for each head and each of the six poses, three sets of 2 000 000 points were merged into a single cloud of 6 000 000 points. At the scale of the entire experiment, this meant merging 3 sets × 6 poses × 35 scanners, yielding 210 *.las files. Next, the geometric consistency of the acquired point clouds was checked for all Livox MID-360 heads in all angular poses using CloudCompare.

Within the data analysis, the first step was to examine the repeatability and internal consistency of the acquired data for all measurements performed with the Livox MID360 heads. For this purpose, the cloud at an orientation of 0 degrees for the first examined head was taken as the reference, and the remaining measurements were registered to it. As the data consistency criterion, the distance between clouds of ±2 cm at 10 m was adopted and, proportionally, ±3.6 cm on the end walls of the laboratory located at a distance slightly above 18 m from the measurement station. Additionally, the symmetry of the

distribution of differences between the data on horizontal and vertical surfaces was examined.

The merged sets for each pose were saved to *.las files (the *.laz format is not supported by Leica Cyclone), following the naming scheme: scanner_serial_number_angle(XXX). Each file contained 6 million points. The cloud for scanner 47MDLA50020047 at an angle of 0° was taken as the reference and labeled, for example, 47MDLA50020047_000_reference.las. The registration of the remaining *.las files to the reference file was carried out in two stages: first manual overlay of the clouds, then "Final register" in CloudCompare with the parameters: RMS difference 1.0E−06, final overlap 90%, random sampling limit 1,000,000, with the "Enable farthest points removal" option activated (Fig. 6).

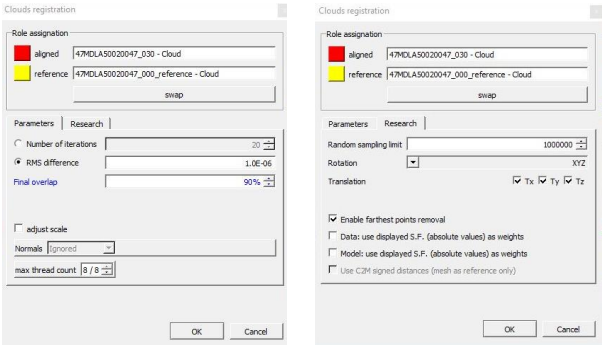

a) b)

Figure 6. Parameters of point cloud orientation in CloudCompare: a) parameters for RMS, b) Parameters for Research

As a result of this stage of work, full repeatability of the acquired geometry was found within the scanner's declared accuracy for all heads in all measurement poses.

Next, the measurement data were imported into Leica Cyclone. The point clouds from the Livox MID-360 heads were registered to the reference cloud from the Leica P40 scanner. For each measurement, an orientation report with accuracy parameters was saved.

The next step of the study was to examine the accuracy of the acquired geometry based on the reference point cloud from the Leica P40 scanner. In this case, due to the demonstrated consistency of the data from the Livox scanners, the assessment was carried out on a representative sample of 40 *.las files (all rotations for one head and one measurement, shifted by the next angle, for the remaining heads).

2.4. Registration to the reference cloud

Due to the magnitude of measurement noise, it turned out that for data from the Livox MID360 scanner, the RANSAC algorithm is unable to fit the reference spheres defined in the software (diameter 0.10 m), regardless of the distance between the sphere and the scanner head. This weakened the geometry of the tie-point network between the tested heads' clouds and the reference point cloud from the Leica P40 scanner.

As a result, registration to the reference cloud was performed on 11 well-identifiable targets on the walls, pedestal, pillars, and ceiling, additionally using a Cloud-to-Cloud constraint. The registration procedure included the following steps:

- perform an initial registration on 11 well-identifiable black-and-white measurement targets;
- add a Cloud-to-Cloud constraint with the following Cloud constraint parameters:
    - search distance 0.04 m (2× the scanner's accuracy);
    - 70% of the point cloud,
    - 500 iterations,
    - start from the current orientation;
- compute the registration and sort results by errors;
- exclude from the registration all targets with an error greater than 5 mm—incorrect identification of the target center due to measurement noise and the point density of the Livox MID360 heads;
- perform optimization of the Cloud-to-Cloud constraint, recompute the registration, and check the results;
- enable/disable targets in the adjustment after analyzing the errors, maintaining the 5 mm error condition;
- iterate the procedure until the accuracy parameters of the adjustment stabilized.

The above procedure made it possible to eliminate target centers that were identified with insufficient accuracy in the data from the Livox heads. These points were identified manually. Here, as with the reference spheres, the automatic identification algorithm could not handle the data from the tested heads. Unfortunately, manual insertion of the vertex means it must be placed at a recorded point of the cloud whose position does not necessarily coincide with the true center of the target; additionally, despite visual control of the vertex insertion point, there is a possibility of assigning it to a point that is not the spatially nearest to the target center.

In the Leica Cyclone preferences, the parameters for saving transformation results were defined as follows: number of decimal places for coordinates and distances: 3 places; for angles: 4 places; for undefined values: 8 places. These parameters followed from the properties of CloudCompare regarding the definition of the translation vector, rotation matrix elements, and angle when entering transformation data for point clouds. Saving from the registration report with accuracy parameters—after the head name (Fig. 7).

```
Status: VALID Registration

Mean Absolute Error:

   for Enabled Constraints = 0.003 m

   Objective Function Value: 0.000102497 sq m
   Iterations: 65
   Overlap Point Count: 271720
   Overlap Error Statistics
     RMS: 0.0110032 m
     AVG: 0.00891038 m
     MIN: 3.97566e-07 m
     MAX: 0.0380784 m
   Overlap Center: (-2.289, -1.225, 1.195) m
   Error after global registration: 1.58044e-05 sq m
   Translation: (-1.610, -0.203, -0.791) m
   Rotation: (0.03558765, -0.01528474, 0.99924967):75.7629 deg

ScanWorld Transformations
Station-001_reference: SW-001 (Leveled)
translation: (0.000, 0.000, 0.000) m
rotation: (0.00000000, 1.00000000, 0.00000000):0.0000 deg

47MDL9Q0020176_030
translation: (-1.605, -0.203, -0.792) m
rotation: (0.03571300, -0.01514890, 0.99924726):75.7649 deg
```

Figure 7. Excerpt of the registration report to the reference cloud with transformation parameters

https://doi.org/10.5194/isprs-archives-XLVIII-1-W6-2025-147-2025

The reference cloud from the Leica scanner (station 1, subsampling 2 mm) and the raw *.las file from the Livox MID-360 head were loaded into CloudCompare. The transformation consistent with the Leica Cyclone report was applied to overlay the Livox cloud onto the reference cloud without additional registration. A local coordinate system with axes parallel to the room walls (X to the longer walls, Y to the shorter) was assigned to both clouds by performing a rotation of 104.5776°, so as to unify the orientation of the data sets and ensure consistent comparisons. The Cloud-to-Cloud distance was then computed with decomposition into X, Y, and Z components, without using additional parameters, yielding differences relative to the reference cloud for each point. The data were filtered to homogeneous wall and ceiling planes: noise and artifacts were removed, leaving only points lying on the structural planes, which made it possible to avoid disturbance of the point distribution by the edge effect, noise from highly reflective objects, etc. (Fig 8-10).

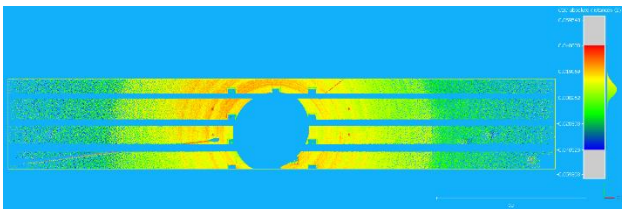

Figure 8.C2C - absolute distance Z

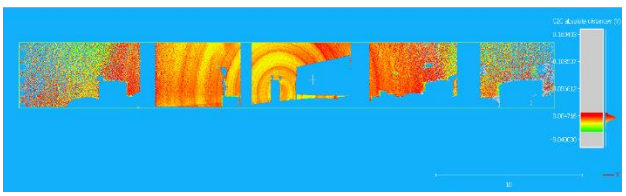

Figure 9. C2C - absolute distance Y

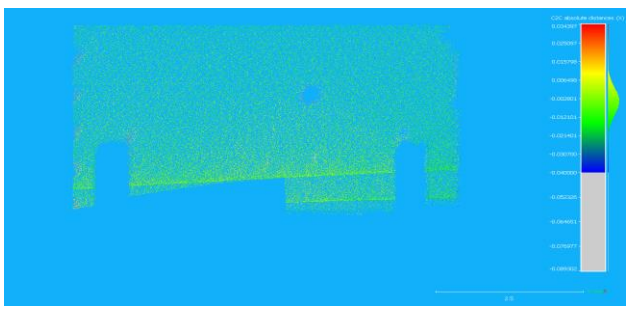

Figure 10. C2C - absolute distance X

In the next step, rasterization of each wall and the ceiling was carried out with a cell size of 0.25 m using the scalar value "Cloud distance X/Y/Z" in accordance with the principal projection direction of the given plane. The projection direction was set orthogonal to the given surface, and the values of the "cell height" attribute and the scalar field were averaged within cells; empty cells were left unfilled. The rasterization result was exported to a point cloud and then saved to a text file with a space separator and column labels.

The text files were opened in a spreadsheet to produce plots for analyzing the distribution of differences between the tested cloud and the reference cloud. For each cloud, at least five sets of plots were prepared: Z, Y1, Y2, X3, X4, corresponding to the ceiling and the individual walls analyzed separately. In the first step, the spatial distance for each point of the resulting cloud from the rasterization process was calculated with respect to the Livox MID-360 head, and then plots were compiled of "spatial distance" as a function of the Cloud-to-Cloud distance for the selected scalar component, which made it possible to assess the distribution of differences for each plane.

Due to the scale of the analyses (40 files × 5 distributions = 200 plots), ChatGPT (model GPT-5) was used to automate plot generation. The AI tool was used solely to prepare repeatable computational scripts and visualization templates; the selection of methodology, interpretations, and conclusions was carried out by the authors. Every generated script/plot was manually verified.

2.5. Results analysis – interpretation of the obtained distributions

As a result of assessing the geometric quality of Livox MID-360 data against the Leica P40 reference cloud, based on the Cloud-to-Cloud (C2C) distance, error distributions were determined for the X (Fig. 11), Y (Fig. 12), and Z (Fig. 13) components. The analysis covers error distributions computed for individual walls after rasterization (measurement areas in the given direction), with decomposition into components and control of dependence on the distance from the head. The interpretation focuses on the error level and its variability.

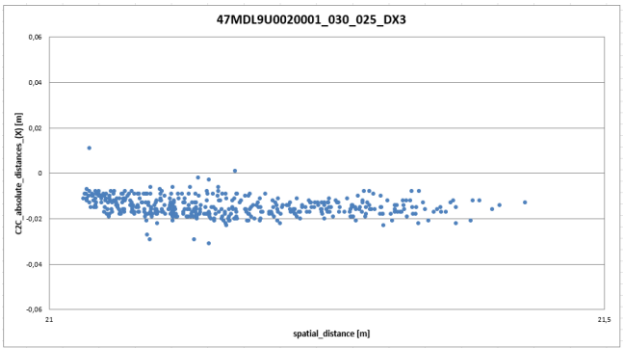

a)

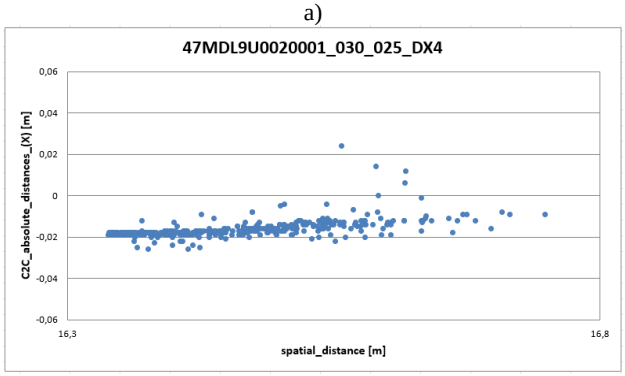

b)

Figure 11. Error distribution in the X direction for two opposite measurement areas: (a) first wall, (b) opposite wall; the scanning head located between the areas.

The error in the X direction was analyzed for two opposite, coaxially aligned walls, with the scanning head in the middle (left and right walls as extreme objects). Across the entire distance range, no variability of the error value was observed; the plots show a linear distribution without a trend. The error range falls within the distance measurement accuracy declared by the manufacturer.

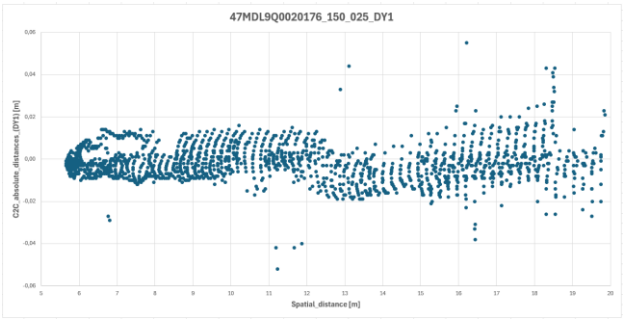

a)

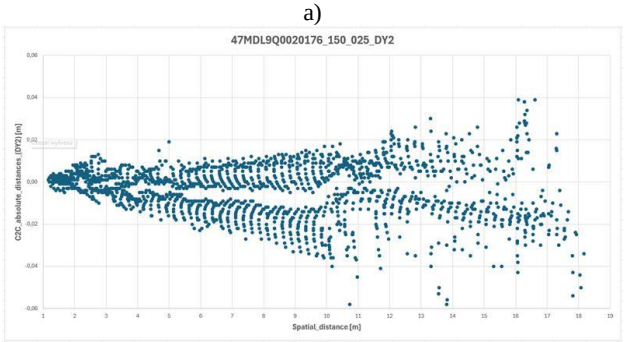

b)

Figure 12. Error distribution in the Y direction for two opposite measurement areas: (a) first wall, (b) opposite wall; the scanning head located between the areas.

The error in the Y direction was analyzed for two opposite, coaxially aligned walls, with the head in the middle. The error values are noticeable and locally inconsistent along the X axis (the direction of the wall length), although they fall within the accuracy range declared by the manufacturer. Both plots refer to the same point cloud. As can be seen (Fig. 12b), the error distribution depends on the horizontal scanning angle; therefore, the characteristic of the error distribution differs in particular directions.

The analysis in the Z direction refers to a common station orientation and a uniform reference surface; we compare the scanning heads. The aim was to assess the consistency and variability of the Z component and to identify any constant offsets between individual units. The error distribution plots for the respective scanners are shown in Fig. 13.

Both heads exhibit the same error behavior in the Z direction. Fluctuations with a near-sinusoidal course fall within the accuracy limits declared by the manufacturer. Changes in error magnitude are likely correlated with the incidence angle of the beam on the surface, which requires further verification. An analysis decomposed by horizontal angles and scanning head directions is recommended.

The analysis revealed the presence of a systematic geometry measurement error for all examined Livox MID-360 heads. This error manifests as a change in the Z-coordinate value most often in the range of 10–12 m from the scanner and is visible on the distribution plots for all analyzed sets.

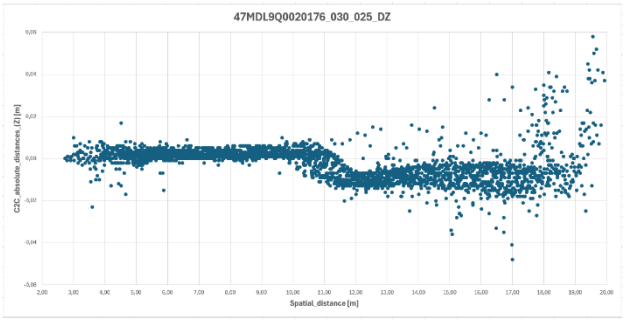

a)

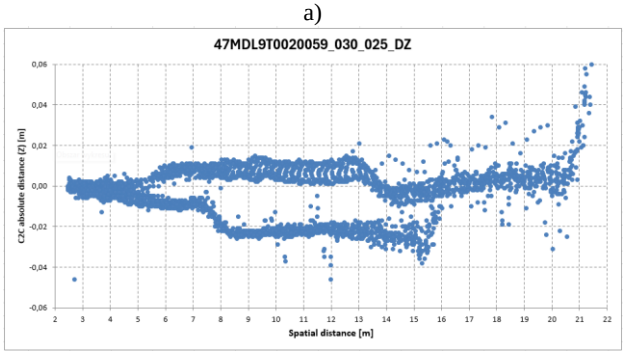

b)

Figure 13. Distribution of the Z-coordinate error for the Livox MID360 head: (a) Head no.76; (b) Head no. 059

3. Results

The obtained results confirmed that the data fall within the distance measurement accuracy declared by the manufacturer, i.e., ±2 cm at 10 m, which indicates correct operation of the heads under laboratory conditions and suitability for tasks requiring centimeter precision. At the same time, a step change in distance relative to the reference cloud was identified most often at a distance of 10–12 m from the scanner head, although this is not a rule for all heads in all directions (e.g., Fig. 12b), which in mobile applications may result in a "banana" error and distort the geometry of the trajectory and the representation of surfaces.

The distance distributions are not symmetrical, and the position of the "step" relative to the reference differs between directions, which justifies decomposing the analysis by directions and evaluating the course of the phenomenon along the longer axis of the laboratory (the X axis of the local coordinate system, retaining the sign from −Xmax to +Xmax). The most probable cause of the "step" is the dependence of error magnitude on the incidence angle of the beam on the surface; for walls analyzed in the X direction the phenomenon was not observed, which indicates the role of observation geometry. From a practical standpoint, the results suggest the need for directional error analysis and inclusion of the incidence angle in calibration procedures and reconstruction algorithms to limit the impact of the identified effect on the final quality of models.

In the X direction, the position error did not exhibit significant variability across the entire analyzed range and fell within the accuracy limits declared by the manufacturer. The examined surface was far from the scanner station and had small linear dimensions, which yielded an incidence angle close to 90°. Under these conditions, the position error resulted mainly from distance measurement error and, to a lesser extent, from random

noise and edge artifacts, which were not the subject of analysis here (discussed in Mitka et al. 2024).

In the Y direction, for two opposite walls analyzed on the same point cloud, different error characteristics were observed: for wall Y1 the values were consistent and showed small fluctuations across the entire distance range, whereas for wall Y2 two distinct characteristics appeared depending on the sign of the X coordinate (from −X to 0 and from 0 to +X). The consistency of results for Y1 and the nature of the discrepancies exclude the influence of a registration error between the tested and reference clouds and indicate a directional inconsistency of information acquisition. Analyses of the remaining heads confirmed this observation.

In the Z direction, a step change in the position error value was found, present in all examined cases, while the error distribution was not fully repeatable. The magnitude of this change was clearly greater than that observed for the Y direction, which confirms its significance for further analyses and applications.

Fig. 14 presents a compilation of error distributions in the Z direction for different heads and different orientations of the head relative to the measurement area. Selected, representative cases from among the 210 analyzed configurations are shown. The set serves to present the results of comparing the nature of Z-direction errors between units and settings under comparable measurement conditions.

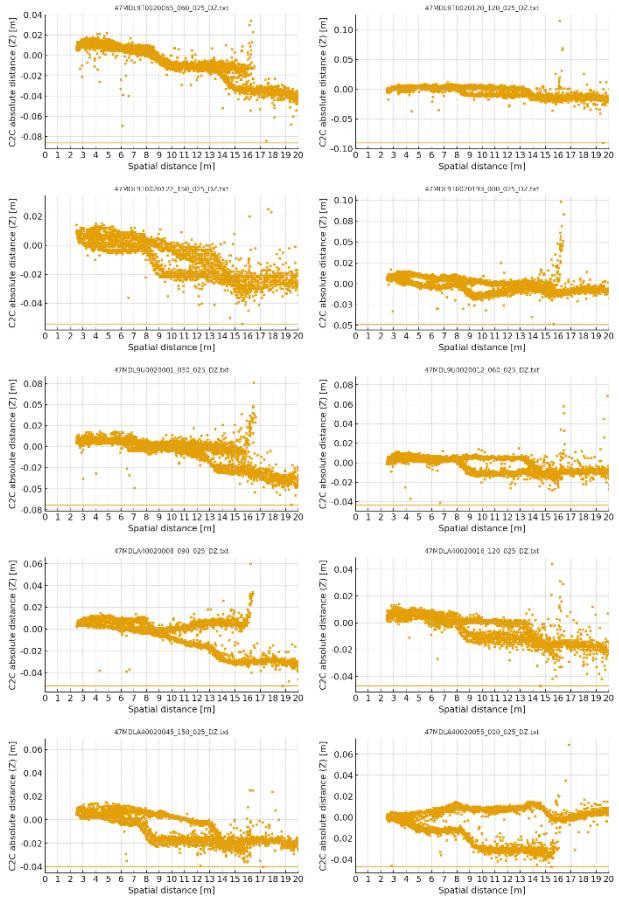

Figure 14. Compilation of error distributions in the Z direction for different heads and different orientations of the head relative to the measurement area.

For the X and Y directions, the error distributions exhibit an analogous character. Minor inconsistencies are local and do not form a clear trend. Overall, the results fall within the accuracy limits declared by the manufacturer.

4. Plan of further research

Subsequent research will include an unambiguous separation of the influence of the distance from the scanner and the incidence angle of the beam on the observed deformation, including the phenomenon of a step change in error. The plan assumes repeating acquisitions with different heads and expanding the measurement geometry, while maintaining the existing processing and evaluation procedure. Several measurement series are planned. In the first series, registration in the laboratory from the center at different heights (different distances from the ceiling) is envisaged. Such a configuration will allow verification of whether the break in the deformation function depends primarily on linear distance or on the incidence angle of the beam on the reference plane. The second series will include measurements from the end of the laboratory in order to analyze the behavior of the deformation function up to a distance of 40 m, also at different heights. This will make it possible to determine the threshold at which—due to an unfavorable incidence angle—the return signal disappears and data quality deteriorates. The third series will be carried out on the shorter wall of the laboratory, moving the scanner along the longer axis every 5 m (from 5 to 35 m). In this configuration, the incidence angle will be close to 90°, and the angular measurement range will decrease with increasing distance, which will allow separation of the influence of distance itself from the influence of the beam incidence geometry on the observed "step."

Further work will focus on analyzing the dependence of error on the incidence angle and distance, decomposition by horizontal angles and scanning directions, verification between individual head units on different surfaces, and modeling and calibration of the systematic error component, including both static and dynamic tests.

5. Conclusions

Laboratory tests confirmed that Livox MID-360 heads deliver data consistent with the manufacturer-declared accuracy (±2 cm at 10 m), which was verified against the TLS reference cloud (Leica P40) for 35 units and yielded consistency across the entire set. At the same time, small, direction-dependent inconsistencies of error distributions and a component with a near-sinusoidal course relative to the reference were noted; these phenomena co-occur with artifacts and random noise, do not violate the declared accuracy, but require consideration when designing processing procedures.

The presented procedure (registration to the reference cloud, Cloud-to-Cloud comparison with X/Y/Z decomposition, 0.25 m rasterization) proved effective and scalable for the assessment of 35 Livox MID-360 heads. The achieved accuracy falls within the manufacturer's declarations (Livox Mid-360 User Manual, v1.2, 2024), which confirms the sensor's suitability for centimeter-precision tasks and is consistent with earlier reports on the applicability of low-cost lidars in engineering applications (Ortiz et al. 2019; Mitka et al. 2024; Balestra et al. 2024). At the same time, direction-dependent differences in distributions and a step change of the error component in the

individual X, Y, Z directions at a distance of approx. 10–15 m were demonstrated, which should be taken into account in quality control and in plane fitting and height reconstruction (Glennie and Hartzell, 2020; Bendkowski et al. 2025).

The observed directional effects and the step in Z should be interpreted as the result of the interaction of scanning geometry with the non-repetitive beam pattern and the incidence angle, which is consistent with the conclusions of studies on the stability and calibration of low-cost sensors (Glennie et al. 2016; Glennie and Hartzell, 2020). A practical consequence (only in the case of measurement error values higher than those declared by the manufacturer) is the need to weight observations with respect to direction and distance and to exercise caution and verify results at large incidence angles, especially in registration and SLAM tasks, where the choice of model and algorithm parameters affects robustness (Lin and Zhang, 2020; Wang et al. 2021). Consistency with field results reported for forestry applications and handheld systems indicates that the MID-360 can be safely used in mapping and inventories, provided that the processing chain includes quality control and verification of the obtained results (Balestra et al. 2024; Mitka et al. 2024; Wu et al. 2023).

The increasing availability and use of low-cost sensors in measurement systems require a systematic assessment of their characteristics in order to maintain reliability, accuracy, and overall result quality. It is necessary to develop and apply uniform test protocols with a reference cloud, covering static and dynamic conditions, various distances, and diverse scanning directions. Consistency and repeatability of data over time should be investigated, as well as sensitivity to scene geometry (including the incidence angle of the beam), variability between units, and the impact of filtering and processing parameters. It is advisable to create error budgets and simple uncertainty models that can be transferred to calibration procedures and observation weighting in practical applications. For reproducibility, it is worth publishing test datasets, scripts, and full assessment reports, which will facilitate device comparisons and accelerate the implementation of best practices.

References

Balestra, M., Cabo, C., Murtiyoso, A., Vitali, A., Alvarez-Taboada, F., Cantero-Amiano, A., Bolaños, R., Laino, D., Pierdicca, R., 2024. Advancing forest inventory: a comparative study of low-cost MLS lidar device with professional laser scanners. *Int. Arch. Photogramm. Remote Sens. Spatial Inf. Sci*., XLVIII-2/W8-2024 (8th International ISPRS Workshop LowCost 3D), 12–13 December 2024, Brescia, Italy. doi.org/10.5194/isprs-archives-XLVIII-2-W8-2024-9-2024

Będkowski, J., Pełka, M., Majek, K., Matecki, M., 2025. Method for spherical camera to 3D LiDAR calibration and synchronization with example on Insta360 X4 and Livox MID-360. *Int. Arch. Photogramm. Remote Sens. Spatial Inf. Sci.*, XLVIII-1/W4-2025 (EuroCOW 2025, 16–18 June 2025, Warsaw, Poland). doi.org/10.5194/isprs-archives-XLVIII-1-W4-2025-13-2025

Glennie, C., Lichti, D.D., 2010. Static calibration and analysis of the Velodyne HDL-64E S2 for high accuracy mobile scanning. *Remote Sens.*, 2, 1610–1624. doi.org/10.3390/rs2061610

Glennie, C.L., Kusari, A., Facchin, A., 2016. Calibration and stability analysis of the VLP-16 laser scanner. *Int. Arch. Photogramm. Remote Sens. Spatial Inf. Sci*., XL-3/W4, 55–60. doi.org/10.5194/isprs-archives-XL-3-W4-55-2016

Glennie, C.L., Hartzell, P.J., 2020. Accuracy assessment and calibration of low-cost autonomous LiDAR sensors. *Int. Arch. Photogramm. Remote Sens. Spatial Inf. Sci*., XLIII-B1-2020, 371–376. doi.org/10.5194/isprs-archives-XLIII-B1-2020-371-2020

Hu, T., Sun, X., Su, Y., Guan, H., Sun, Q., Kelly, M., Guo, Q., 2021. Development and performance evaluation of a very low-cost UAV-LiDAR system for forestry applications. *Remote Sens*., 13, 77. doi.org/10.3390/rs13010077

Hyyppä, E., Kukko, A., Kaijaluoto, R., White, J.C., Wulder, M.A., Pyörälä, J., Liang, X., Yu, X., Wang, Y., Kaartinen, H., et al., 2020. Accurate derivation of stem curve and volume using backpack mobile laser scanning. *ISPRS J. Photogramm. Remote Sens*., 161, 246–262. doi.org/10.1016/j.isprsjprs.2020.01.018

Lin, J., Zhang, F., 2020. LOAM-Livox: A fast, robust, high-precision LiDAR odometry and mapping package for LiDARs of small FoV. Proc. IEEE ICRA 2020, Paris, France, 31 May–31 August 2020, 3126–3131.

Livox, 2024: Livox Mid-360, *User Manual v1.2*.

Livox, 2025. Livox Mid-360. livoxtech.com/mid-360 (15 October 2025).

Mitka, B., Klapa, P., Gawronek, P., 2024. Laboratory tests of metrological characteristics of a non-repetitive low-cost mobile handheld laser scanner. *Sensors*, 24, 6010. doi.org/10.3390/s24186010

Ortiz Arteaga, A., Scott, D., Boehm, J., 2019. Initial investigation of a low-cost automotive LiDAR system. *Int. Arch. Photogramm. Remote Sens. Spatial Inf. Sci*., XLII-2/W17, 233–240. doi.org/10.5194/isprs-archives-XLII-2-W17-233-2019

Redovniković, L., Jakopec, A., Będkowski, J., Jagetić, J., 2024. The affordable DIY Mandeye LiDAR system for surveying caves, and how to convert 3D clouds into traditional cave ground plans and extended profiles. *International Journal of Speleology*, 53(3), ijs2535. doi.org/10.5038/1827-806X.53.3.2535

Wang, Y., Lou, Y., Zhang, Y., Song, W., Huang, F., Tu, Z., 2021. A robust framework for simultaneous localization and mapping with multiple non-repetitive scanning Lidars. *Remote Sens*., 13, 2015. doi.org/10.3390/rs13102015

Wu, W., Li, J., Chen, C., Yang, B., Zou, X., Yang, Y., Xu, Y., Zhong, R., Chen, R., 2023. AFLI-Calib: Robust LiDAR-IMU extrinsic self-calibration based on adaptive frame length LiDAR odometry. *ISPRS J. Photogramm. Remote Sens*., 199, 157–181. doi.org/10.1016/j.isprsjprs.2023.04.004